A Gamma-Ray Periodic Modulation in Globular Cluster 47 Tucanae

Peng-Fei Zhang[1,2], Jia-Neng Zhou[3], Da-Hai Yan[4,5,6], Jing-Zhi Yan[2,7], Yi-Zhong Fan[2,7], Jun Fang[1], and Li Zhang[1]

[1] Department of Astronomy, School of Physics and Astronomy, Key Laboratory of Astroparticle Physics of Yunnan Province, Yunnan University, Kunming 650091, People's Republic of China; zhangpengfei@ynu.edu.cn, fangjun@ynu.edu.cn
[2] Key Laboratory of Dark Matter and Space Astronomy, Purple Mountain Observatory, Chinese Academy of Sciences, Nanjing 210034, People's Republic of China
yzfan@pmo.ac.cn
[3] Shanghai Astronomical Observatory, Chinese Academy of Sciences, 80 Nandan Road, Shanghai 200030, People's Republic of China; zjn@shao.ac.cn
[4] Key Laboratory for the Structure and Evolution of Celestial Objects, Yunnan Observatory, Chinese Academy of Sciences, Kunming 650011, People's Republic of China
[5] Center for Astronomical Mega-Science, Chinese Academy of Sciences, 20A Datun Road, Chaoyang District, Beijing 100012, People's Republic of China
[6] Key Laboratory for the Structure and Evolution of Celestial Objects, Chinese Academy of Sciences, Kunming 650011, People's Republic of China
[7] School of Astronomy and Space Science, University of Science and Technology of China, Hefei, Anhui 230026, People's Republic of China
Received 2020 September 2; revised 2020 October 25; accepted 2020 November 3; published 2020 December 2

Abstract

The globular cluster 47 Tucanae was first detected in gamma rays by the Large Area Telescope (LAT) on board the Fermi Gamma-ray Space Telescope, and the gamma-ray emission has been widely attributed to the millisecond pulsars. In this work, we analyze the Fermi-LAT pass 8 data ranging from 2008 August to 2017 May and report the detection of a modulation with a period of 18.416 ± 0.008 hr at a significance level of $\sim 4.8\sigma$. This is the first time detecting a significant modulation with a period much longer than that of millisecond pulsars in gamma rays from globular clusters. The periodic modulation signal appears in the Swift Burst Alert Telescope (BAT) data as well. The phase-folded Chandra X-ray light curve of a point source may have provided an additional clue.

Unified Astronomy Thesaurus concepts: Globular star clusters (656); Gamma-rays (637); Binary pulsars (153); Periodic orbit (1212)

1. Introduction

With ages greater than 10^{10} yr, globular clusters (GCs) are the oldest spherical, self-gravitating aggregations of stars orbiting the bulge of a host galaxy. More than 150 GCs are detected in the Milky Way with radio and/or optical detectors (Harris 1996). 47 Tucanae (henceforth 47 Tuc), located at a distance of ~ 4.0 kpc from the Earth, was first detected in gamma rays by the Fermi Large Area Telescope (LAT; Abdo et al. 2009a; Atwood et al. 2009). The spectral energy distribution (SED) is similar to that of millisecond pulsars (MSPs; Grindlay et al. 2001; Abdo et al. 2009a; Freire et al. 2011). Interestingly, 25 MSPs have been identified in 47 Tuc, and the total number is estimated to be >30 (Grindlay et al. 2001; Heinke et al. 2005; Abdo et al. 2010). So far 16 gamma-ray GCs and several candidates have been reported, and all of the gamma-ray spectra resemble those of MSPs (Abdo et al. 2010; Kong et al. 2010; Tam et al. 2011b; Acero et al. 2015; Zhou et al. 2015; Zhang et al. 2016). Together with the detection of millisecond gamma-ray pulsations from a young MSP J1823−3021A in NGC 6624 (Freire et al. 2011) and PSR B1821−24 in M28 (Wu et al. 2013), these facts strongly favor the hypothesis that the GeV emission of 47 Tuc or even all GCs mainly comes from a large population of MSPs.

GCs likely host other kinds of gamma-ray emitters as well. Owing to the high stellar density and hence the large stellar encounter rate, GCs are expected to host low-mass X-ray binaries (LMXB, the progenitors of MSPs; Clark 1975; Alpar et al. 1982; Cheng & Taam 2003; Liu et al. 2007) and binary MSPs. Several binary MSPs, including Black Widow and Redback binary systems, are identified as gamma-ray emitters (Guillemot et al. 2012; Wu et al. 2012; Xing & Wang 2015). So far there are 15 known MSP binaries, including 5 quiescent LMXBs and 1 black hole LMXB, already detected in 47 Tuc by radio, optical, and X-ray telescopes (Heinke et al. 2005;

Miller-Jones et al. 2015). A new gamma-ray emission component with periodic modulation of hours may thus be present, which motivates us to reanalyze the gamma-ray emission from 47 Tuc.

2. Fermi-LAT Data Analysis

We construct the LAT light curve using a modified version of aperture photometry with 500 s time bins for 47 Tuc. We extract events within a circular region with a radius of $\sim 3°$ centered on the location of 47 Tuc in the energy range from 100 MeV to 500 GeV. Using the tool *gtmktime*, we select the good time intervals (GTIs) to exclude the periods when 47 Tuc was close to the Earth's limb or within $5°$ of the Sun and the Moon. Because a time-bin of 500 s is shorter than the sky survey rocking period of Fermi-LAT, the large exposure changes from time-bin to time-bin for 47 Tuc. So we use the tool *gtexposure* to determine exposure for each time-bin. Then photon arrival times are barycenter corrected using the tool *gtbary*. We also use the tool *gtsrcprob* to assign probabilities for each event basing on the new generated model file. The light curve is calculated by summing the probabilities of events (rather than the number of photons to remove the possible contamination of nearby sources) and weighting the relative exposures of each time-bin. Similar approaches are widely adopted in the literature (Corbet et al. 2007; Abdo et al. 2009b; Ackermann et al. 2012). The details of our data reduction are introduced in the Appendix.

We calculate the power spectrum for the entire light curve after subtracting the mean flux to examine the possible periodic modulation with the method of a Lomb–Scargle periodogram (Lomb 1976; Scarle 1982). The power spectrum is shown in Figure 1 and displays a distinct peak at 1.3032 ± 0.0003 day^{-1} (~ 18.42 hr). The probability (p_{prob}; Lomb 1976; Scarle 1982) of obtaining power from the chance fluctuation (the noise)
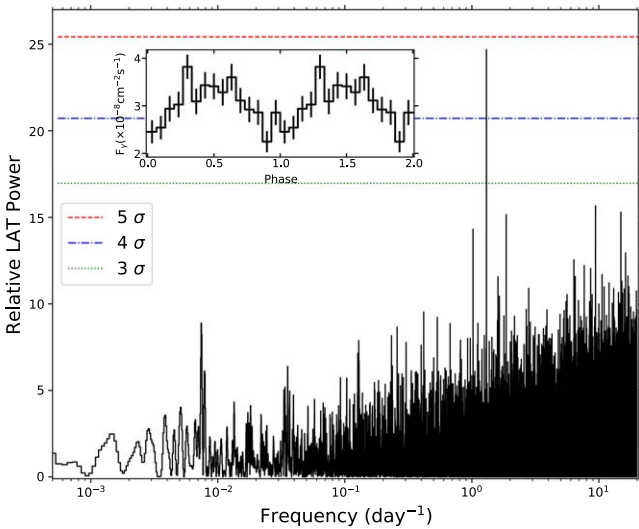
Figure 1. Power spectrum calculated from gamma-ray light curve of 47 Tuc. The light curve is obtained with the aperture photometry method for the data above 100 MeV with the time-bin of 500 s. The green dotted, blue dashed–dotted, and red dashed horizontal lines represent 3σ, 4σ, and 5σ confidence levels, respectively. The inset plot shows the phase-resolved light curves folded with the period.

equal to or larger than the power spectral peak is $<1.8 \times 10^{-11}$. Taking into account the number of statistically independent frequency trials (N), the false-alarm probability (FAP) is $<1.15 \times 10^{-6}$. And the FAP (Scarle [1982]) is calculated as $\mathrm{FAP} = 1 - (1 - p_{\mathrm{prob}})^N$. The significance of the power spectral peak is estimated to be at $\sim 4.8\sigma$ (99.999885%) confidence level. In Figure [1], we also show 3σ, 4σ, and 5σ confidence levels with green dotted, blue dashed–dotted, and red dashed lines, respectively.

As shown in panel (A) of Figure [A2] in the [Appendix], there is no significant emission above 50 GeV for 47 Tuc. To increase the signal to noise of the target, we reanalyzed the Fermi-LAT events with data up to 50 GeV, and the significance increases up to 4.9σ. More intriguingly, if we limit the data up to ~ 5 GeV, the significance increases to 5.2σ and the power spectrum is shown in Figure [A1] in the [Appendix]. To check whether our signal detected in 47 Tuc is artificial or not, we also extract light curves with the same method for bright gamma-ray sources around 47 Tuc in 3FGL (Acero et al. [2015]), then calculate their power spectra. No similar signal has been identified. We further analyze the data of LS 5039, LS I +61°303, Cygnus X-3, 1FGL J1018.6−5856, and CXOU J053600.0−673507, and we confirm the signals (including their periods and the significance) reported in the literature (Abdo et al. [2009b], [2009c], [2009d]; Ackermann et al. [2012]; Corbet et al. [2016]). We then conclude that our signal is robust and create phase-resolved fluxes employing likelihood analysis within each phase-bin for gamma rays (see the upper panel of Figure [2]).

3. Summary and Discussion

Gamma-ray orbit modulation has been detected in some high-mass X-ray binaries (HMXBs; Abdo et al. [2009c], [2011]; Tam et al. [2011a]; Ackermann et al. [2012]; Corbet et al. [2016]). Our localization of the emission in the high state yields an error circle of $\sim 0°.034$ that covers 47 Tuc. The superposition of an

HMXB in such a small field of view is thus unlikely, and we do not discuss such a scenario further.

An alternative and attractive possibility is that one of the MSP binaries (either the Redback or Black Widow system) in 47 Tuc radiates significantly in gamma rays. The orbital periods of the 15 MSP binaries in 47 Tuc (Heinke et al. [2005]; Miller-Jones et al. [2015]), inferred from radio and optical observations, span several hours to several days. Our gamma-ray modulation period ~ 18.4 hr is indeed within such a range. However, none of the currently known MSP binaries in 47 Tuc has an orbital period of ~ 18.4 hr, possibly indicating the presence of more MSP binaries in this source.

To further check this possibility and also identify the possible counterpart for the modulation, we have analyzed the Swift-BAT data, and found a signal with almost the same orbital period as the gamma-ray modulation at a local significance level of $\sim 4.5\sigma$ (see the [Appendix] and Figure [A3]). We have analyzed the Chandra X-ray data from two Chandra ACIS detectors, and found an interesting source at coordinates of R.A. $= 00^{\mathrm{h}}24^{\mathrm{m}}06\overset{\mathrm{s}}{.}389$ and decl. $= -72°04'43''.006$ (i.e., CXOGlb J002406.3−720443; see the [Appendix] and Figure [A4]). The Chandra X-ray observations are not dense enough, and the longest individual observation is less than 20 hr. Consequently, the power spectrum at the frequencies of interest is not well defined with such short observations. We therefore do not display its power spectrum analysis. The X-ray folded light curve after removing the influence of two flares is shown in the lower panel of Figure [2]. Interestingly, the phase-resolved gamma-ray and X-ray light curves have a similar shape. More importantly, the folded gamma-ray and X-ray light curves both reach their maximum in the fifth phase-bin. We thus take CXOGlb J002406.3−720443 as the candidate of the source of our periodic gamma-ray signal. Motivated by these facts, we conclude that there is a new gamma-ray emitter, possibly an MSP binary, in 47 Tuc.

Note that PSR 1957+20 (Wu et al. [2012]) and PSR J1311-3430 (Xing & Wang [2015]), two Black Windows, show orbital modulations in gamma rays. The orbital phase offset between X-ray and gamma-ray modulations suggests that their gamma rays are produced by inverse Compton scattering (Cheng et al. [2006]; Tam et al. [2011a]; Ng et al. [2018]; Clark et al. [2020]), rather than the synchrotron of electrons, which is considered as the origin of the X-ray radiations (Bogdanov et al. [2005]; An et al. [2018], [2020]). While in 47 Tuc, the gamma-ray orbital modulation has the same orbital phase as the X-ray modulation, suggesting that this gamma-ray component from 47 Tuc is produced by synchrotron emission from particles accelerated along the shock front, same as the origin of the X-ray emissions.

The phase-resolved spectral properties and fluxes for maximum (phase-bin 5) and minimum (phase-bin 14) are listed in Table [A1] in the [Appendix]. We find that the maximum spectrum ($\Gamma_{\mathrm{H}} = 1.82 \pm 0.13$) is softer than minimum one ($\Gamma_{\mathrm{L}} = 1.26 \pm 0.25$). The difference of Γ is 0.56 ± 0.28. This suggests the orbitally varying component expected in the intrabinary shock emission models, and a similar scenario is also discussed in An et al. ([2018]). Dedicated X-ray and optical observations are encouraged/needed to finally reveal the nature of the gamma-ray periodic modulation in 47 Tuc.
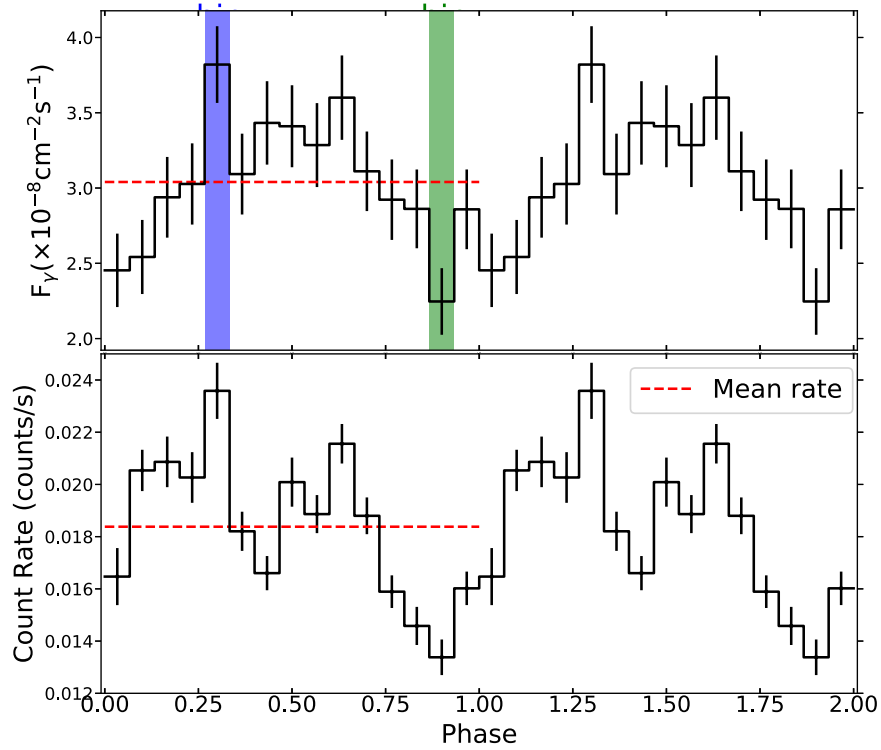
Figure 2. Phase-resolved light curves (two cycles are shown for clarity). Upper panel: the gamma-ray flux intensity pulse shape folded with a period cycle of 18.416 hr. The red dashed line marks the mean flux. The phase-bins in high and low states are labeled with blue and green vertical bars, respectively. The highest and lowest TS values of the bins are ~549 and ~296, respectively. Lower panel: phase-resolved count rate with data from Chandra X-ray observatory.

Appendix

Gamma-ray data reduction. In the analysis we employ the Science Tools available from the Fermi Science Support Center (FSSC) with software version v10r0p5 package. The Fermi-LAT (Atwood et al. 2009) data used here were observed between 2008 August 8 and 2017 May 20 (modified Julian date, MJD: 54,682.66–57,894.00). We only select photons between 100 MeV and 500 GeV to reduce diffuse emission and improve point-spread function. We exclude the events with zenith angles >90° to minimize the contamination from the gamma-ray-bright Earth limb. The high-quality data (Pass 8 SOURCE class photon-like events with options of *evclass = 128* and *evtype = 3*) are used to obtain the GTIs by running Fermi Science Tools *gtmktime* with a filter expression of "(DATA_QUAL > 0)&&(LAT_CON-FIG==1)." The instrumental response function "P8R2_SOUR-CE_V6," recommended by Fermi-LAT Collaboration, is adopted.

Our region of interest (ROI) is an area of 20° × 20° centered at position of 47 Tuc (J2000; $l = 305.895$, $b = -44.889$). We bin the data into 200 × 200 grid points with a spatial pixel size of $0°.1 \times 0°.1$ in spatial dimensionality and into 30 logarithmically equal bins in energy dimensionality. The two
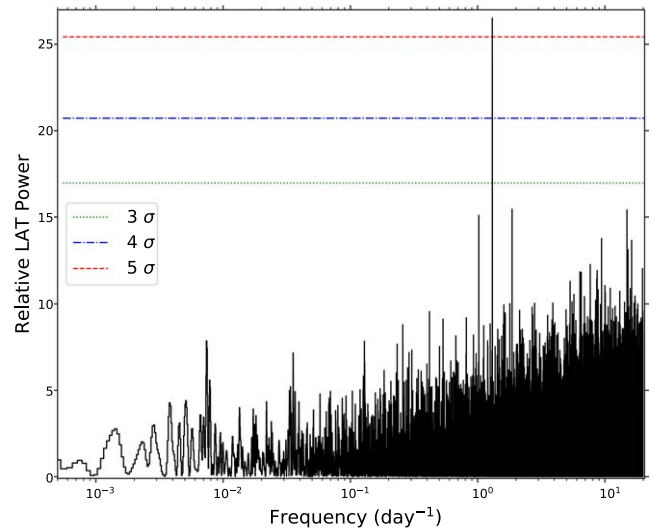

Figure A1. Same as Figure 1, but for the power spectrum calculated from the gamma-ray light curve with data up to ~5 GeV.

latest background components (i.e., gll_iem_v06.fits and iso_P8R2_SOURCE_V6_v06.txt) are adopted to model gamma rays from Galactic diffuse and extragalactic isotropic emissions. The background sources in the ROI are adopted from the Fermi-LAT 4 yr Point Source Catalog (3FGL; Acero et al. 2015). A binned maximum likelihood algorithm packaged in the tool *gtlike* is performed to fit the events with the model file. In the modeling, we free the normalizations and spectral parameters of sources within the radius of 5°, fix the spectral parameters to that reported in 3FGL (Acero et al. 2015) for the sources at the radii between 5° and 10°, and freeze all the
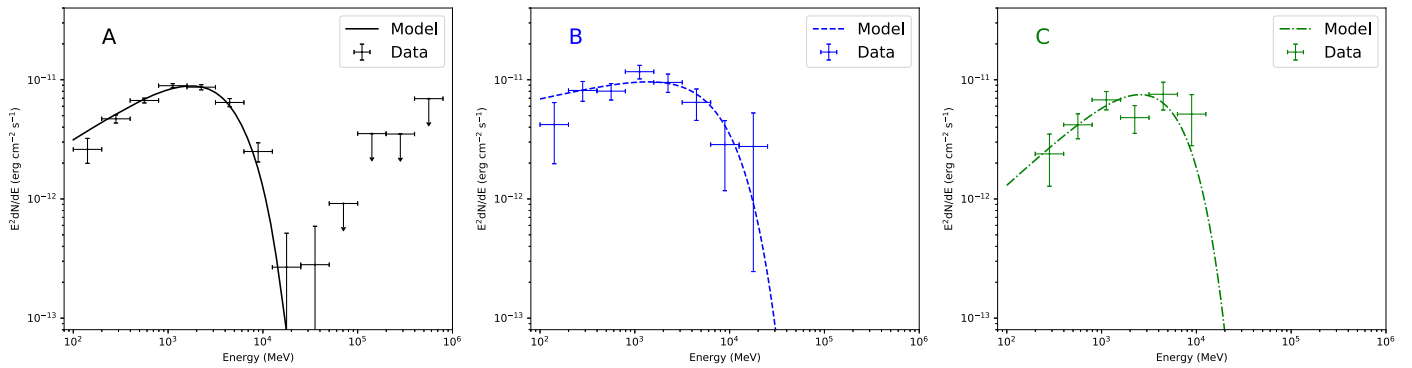
Figure A2. Phase-averaged SED and the ones in high and low state phase-bins are shown in panels (A), (B), and (C), respectively, with the lines indicating the best-fit spectral models in likelihood analysis presented in Table A1. Note that, for panel (A), the TS value of the data point with a large error in 25–50 GeV is ∼4.

parameters for other sources. The exceptions are the highly variable sources with a variability index exceeding 72.44, for which the normalizations are set free, as are the two background components. For 47 Tuc, the spectral shape has a function of a superexponentially cutoff power law ($dN/dE = N_0 E^{-\Gamma} \exp{(-E/E_{cut})^b}$; where the parameters of N_0, E_{cut}, Γ, and b are the normalization factor, the cutoff energy, the photon index, and the sharpness of the cutoff, respectively). Running the tool *gtlike*, we derive the best-fit results, including flux intensities, photon spectral indices, and likelihood ratio test statistic (TS) values. The TS is defined as TS $= -2(\mathcal{L}_0 - \mathcal{L}_l)$, where $\mathcal{L}_0$ and $\mathcal{L}_l$ represent logarithmic maximum likelihood values under the null and alternative model (i.e., without and with the target). The best-fit results are saved as a new model file, which is the base of the following data analysis. Unless otherwise stated, the uncertainties given in this work are the 1σ statistical errors.

A power spectrum is also calculated from the gamma-ray light curve with the Fermi-LAT data < 5 GeV, and the QPO at 18.42 hr is found to have a significance level of 5.2 σ (see Figure A1).

Phase-resolved gamma-ray emission. To investigate the variability on the period cycle of 47 Tuc, we employ the phase-resolved likelihood analysis method to fold the events in the ROI into 15 uniform orbital phase-bins (the zero-point is set at MJD 54,682.66). The phase-resolved spectral properties and fluxes within each phase-bin (Figure 2) are obtained by running the tool *gtlike* with the new model file. We fit the phase-resolved light curve with a constant by employing the χ^2-statistic and have $\chi^2/\text{dof} = 42/14$, which indicates a significant variability. We have derived the phase-resolved SEDs for phase-bins with $4/15 < \phi < 5/15$ and $13/15 < \phi < 14/15$ to examine the difference in high (phase-bin 5) and low states (phase-bin 14) (see the blue and green vertical bars in the upper panel of Figure 2, respectively). The three SEDs (including the phase-averaged one) are shown in panels (A), (B), and (C) of Figure A2, respectively. The lines represent the best-fit results derived by the tool *gtlike*. In Table A1 we summarize our best-fit parameters (the integrated energy flux and isotropic gamma-ray luminosity) of the phase-resolved SED (see Figure A2) of the gamma-ray emission in the ROI. Phase-bin$_{All}$, Phase-bin$_H$, and Phase-bin$_L$ represent the time-averaged and high and low state phase-bins, respectively. The spectrum in the low state is harder than in the high state. The flux difference between "high" and "low" states is $\sim 1.5 \times 10^{-8}$ photons cm^{-2} s^{-1} (corresponding to a luminosity of $\sim 2.80 \times 10^{34}$ erg s^{-1}). And the spectrum in the "low" state is harder than in the "high" state (see Figure A2
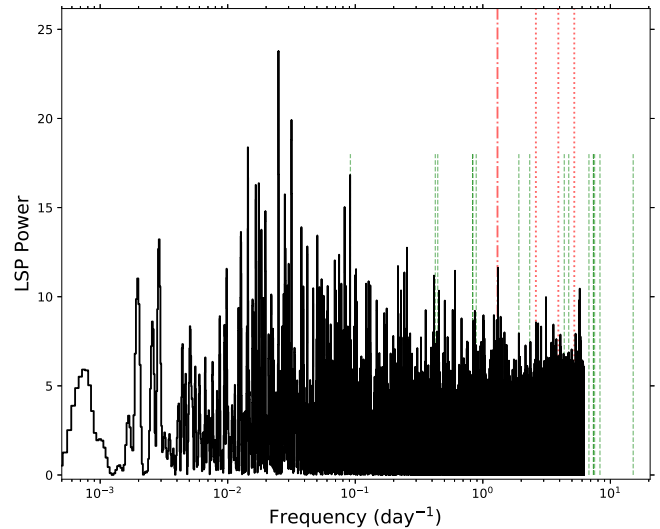

Figure A3. Power spectrum of the Swift-BAT X-ray light curve of 47 Tuc. The red dashed–dotted line indicates the period detected in gamma ray, and the red dotted lines are its second, third, and fourth harmonics, respectively. The shorter green dashed lines indicate the periods of 15 currently known MSP binaries (acquired at http://www.naic.edu/~pfreire/GCpsr.html) in 47 Tuc.

and Table A1). We conjecture that the gamma rays in the "low" state come from a population of isolated MSPs, while the gamma rays in the high state also consist of the peak (periodic) emission of the new source. As shown in, e.g., Xing & Wang (2015, 2016), the emission from isolated MSPs is usually harder than that from the Black Widows/Redback systems. This may help explain the softer spectrum of our signal in the high state.

X-ray emission analysis. To verify our gamma-ray periodic signal and identify the candidate source, we have collected the X-ray archive data of 47 Tuc. A long-term set is provided by the Swift-BAT hard X-ray transient monitor (Barthelmy et al. 2005; Krimm et al. 2013) spanning from MJD 53,416 to 58,134. Its power spectrum is presented in Figure A3. Interestingly, a peak with a local significance of ∼4.5σ (the probability is 99.9992%) is found almost at the same period as that found in gamma rays (see the red dashed–dotted line). Such consistency provides strong support for the periodic modulation signal shown in the Fermi-LAT of 47 Tuc. Since the Swift-BAT data cannot provide accurate location information of the candidate source(s), below we focus on the Chandra (Fruscione et al. 2006) X-ray data that are characterized by the unprecedented angular resolution (Weisskopf et al. 2002).
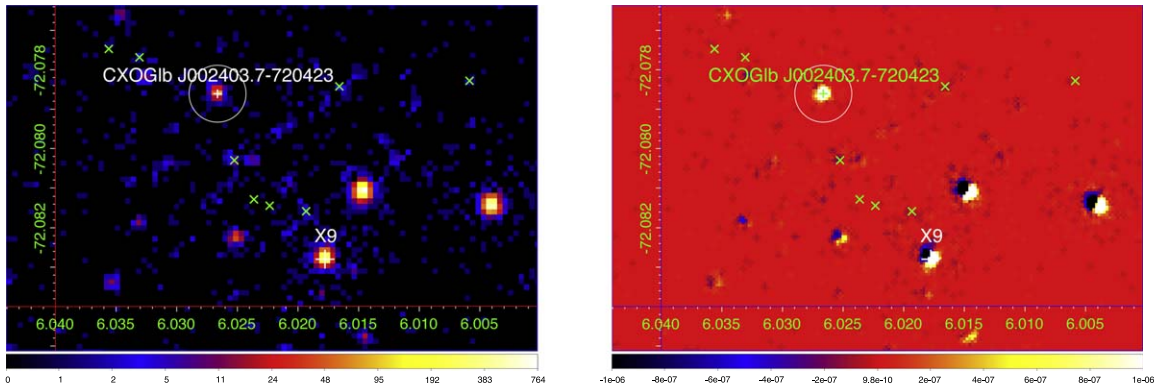
Figure A4. Counts map created with the data of ObsID 955 (left) and the residual map created with the data of ObsIDs 955 and 953 (right). The candidate source (CXOGlb J002406.3–720443) is marked with a cross. A black hole candidate X-ray binary 47 Tuc X9 (R.A. = $00^h24^m04\overset{s}{.}264$ and decl. = $-72^\circ04'58''09$; Miller-Jones et al. 2015; Bahramian et al. 2017) is also marked. And the green crosses indicate the MSPs that have been identified in 47 Tuc.

<div align="center">

Table A1
Results of Phase-resolved Analysis

</div>

Phase-bin	Γ	b	E_{cut} (GeV)	TS Value	f_γ ($\times 10^{-11}$ erg cm^{-2} s^{-1})	L_γ ($\times 10^{34}$ erg s^{-1})
Phase-bin$_{All}$	1.48 ± 0.12	1.14 ± 0.24	3.5 ± 1.1	6196.5	3.01 ± 0.08	5.76 ± 0.16
Phase-bin$_H$	1.82 ± 0.13	$1.14^{(\dagger)}$	6.9 ± 2.8	538.7	3.55 ± 0.27	6.79 ± 0.52
Phase-bin$_L$	1.26 ± 0.25	$1.14^{(\dagger)}$	3.7 ± 1.3	296.3	2.09 ± 0.21	3.99 ± 0.41

Note: Best-fit parameters of phase-resolved likelihood analysis for the time-averaged and high and low state phase-bins. b marked with † are fixed in the likelihood analysis for high and low states phase-bins. f_γ is integrated energy flux. L_γ is isotropic gamma-ray luminosity.

To identify the possible candidates for the gamma-ray modulation with a period of ~18 hr, we create two exposure-corrected images of the observations with the ID numbers of 955 and 953, respectively. Their time interval is both ~10 hr (i.e., about half of the modulation period of our signal). If our gamma-ray periodic modulation is caused by the orbital period of a binary, these two exposure-corrected images (having the same exposure time ~8.8 hr) should cover the flux maximum and minimum of the target, respectively. The digital subtraction is carried out to get the residual map (shown in the right panel of Figure A4), with which we find five bright sources. Our best candidate is spatially consistent with CXOGlb J002406.3–720443, shown in Figure A4 marked with a cross. Its X-ray light curves (0.3–8 keV) are extracted from a circle ROI of ~2$''$6 radius with a time-bin of 4.4 ks for all observations from Chandra ACIS detectors. We fold them with a period cycle of 18.4 hr (zero phase is set at MJD 54,682.66) and present the resulting light curve in the lower panel of Figure 2. Its averaged X-ray energy flux is $(1.29 \pm 0.22) \times 10^{-13}$ ergs cm^{-2} s^{-1}. The gamma-ray-to-X-ray flux ratios are 233 ± 40, 275 ± 52, and 162 ± 33 for the time-averaged and high and low states, respectively. Finally we would like to remark that the nature of CXOGlb J002406.3–720443 is still unclear. It was suggested to be a cataclysmic variable, but an LMXB cannot be ruled out yet (Grindlay et al. 2001).

ORCID iDs

Yi-Zhong Fan ⓘ https://orcid.org/0000-0002-8966-6911

References

Abdo, A. A., Ackermann, M., Ajello, M., et al. 2009a, ApJL, 701, L123
Abdo, A. A., Ackermann, M., Ajello, M., et al. 2009b, Sci, 325, 845
Abdo, A. A., Ackermann, M., Ajello, M., et al. 2009c, ApJ, 700, 597
Abdo, A. A., Ackermann, M., Ajello, M., et al. 2009d, ApJ, 706, 56
Abdo, A. A., Ackermann, M., Ajello, M., et al. 2010, A&A, 524, 75
Abdo, A. A., Ackermann, M., Ajello, M., et al. 2011, ApJL, 736, L11
Acero, F., Ackermann, M., Ajello, M., et al. 2015, ApJS, 218, 23
Ackermann, M., Ajello, M., Ballet, J., Barbiellini, G., et al. 2012, Sci, 335, 189
Alpar, M. A., Cheng, A. F., Ruderman, M. A., & Shaham, J. 1982, Natur, 300, 728
An, H., Romani, R. W., & Kerr, M. 2018, ApJL, 868, L8
An, H., Romani, R. W., & Kerr, M. 2020, ApJ, 897, 52
Atwood, W. B., Abdo, A. A., Ackermann, M., et al. 2009, ApJ, 697, 1071
Bahramian, A., Heinke, C. O., Tudor, V., et al. 2017, MNRAS, 467, 2199
Barthelmy, S. D., Barbier, L. M., Cummings, J. R., et al. 2005, SSRv, 120, 143
Bogdanov, S., Grindlay, J. E., van den Berg, M., et al. 2005, ApJ, 630, 1029
Cheng, K. S., & Taam, R. E. 2003, ApJ, 300, 500
Cheng, K. S., Taam, R. E., Wang, W., et al. 2006, ApJ, 641, 427
Clark, C. J., Nieder, L., Voisin, G., et al. 2020, arXiv:2007.14849
Clark, G. W. 1975, ApJL, 199, L143
Corbet, R. H. D., Chomiuk, L., Coe, M. J., et al. 2016, ApJ, 829, 105
Corbet, R. H. D., Markwardt, C. B., & Tueller, J. 2007, ApJ, 655, 458
Freire, P. C. C., Abdo, A. A., Ajello, M., et al. 2011, Sci, 334, 1107
Fruscione, A., McDowell, J. C., Allen, G. E., et al. 2006, Proc. SPIE, 6270, 62701V
Grindlay, J. E., Heinke, C., Edmonds, P. D., & Murray, S. S. 2001, Sci, 292, 2290
Guillemot, L., Johnson, T. J., Venter, C., et al. 2012, ApJ, 744, 33
Harris, W. E. 1996, AJ, 112, 1487
Heinke, C. O., Grindlay, J. E., Edmonds, P. D., et al. 2005, ApJ, 625, 796
Kong, A. K. H., Hui, C. Y., & Cheng, K. S. 2010, ApJL, 712, 36
Krimm, H. A., Holland, S. T., Corbet,. R. H. D., et al. 2013, ApJS, 209, 14
Liu, Q. Z., van Paradijs, J., & van den Heuvel, E. P. J. 2007, A&A, 469, 807
Lomb, N. R. 1976, Ap&SS, 39, 447
Miller-Jones, J. C. A., Strader, J., Heinke, C. O., et al. 2015, MNRAS, 453, 3918
Ng, C. W., Takata, J., Strader, J., Li, K. L., & Cheng, K. S. 2018, ApJ, 867, 90
Scarle, J. D. 1982, ApJ, 263, 835
Tam, P. H. T., Huang, R. H. H., Takata, J., et al. 2011a, ApJL, 736, L10
Tam, P. H. T., Kong, A. K. H., Hui, C. Y., et al. 2011b, ApJ, 729, 90
Weisskopf, M. C., Brinkman, B., Canizares, C., et al. 2002, PASP, 114, 1
Wu, E. M. H., Takata, J., Chang, K. S., et al. 2012, ApJ, 761, 181
Wu, J. H. K., Hui, C. Y., Wu, E. M. H., et al. 2013, ApJL, 765, L47
Xing, Y., & Wang, Z. X. 2015, ApJL, 804, L33
Xing, Y., & Wang, Z. X. 2016, ApJ, 831, 143
Zhang, P. F., Xin, Y. L., Fu, L., et al. 2016, MNRAS, 459, 99
Zhou, J. N., Zhang, P. F., Huang, X. Y., et al. 2015, MNRAS, 448, 3215